Journal of Advanced Ceramics
2019, **8**(1): 39–46
https://doi.org/10.1007/s40145-018-0289-x
ISSN 2226-4108
CN 10-1154/TQ

Research Article

Preparation and characterization of monodispersed spherical Fe_2O_3@SiO_2 reddish pigments with core–shell structure

Shile CHEN[a,b], Mengting CHENG[b], Ying LANG[a], Chuanjin TIAN[a], Hongkang WEI[a], Chang-An Wang[b,*]

[a]*School of Materials Science and Engineering*, *Jingdezhen Ceramic Institute*, *Jingdezhen 333403, China*
[b]*State Key Laboratory of New Ceramics and Fine Processing*, *School of Materials Science and Engineering*, *Tsinghua University*, *Beijing 100084*, *China*

Received: March 21, 2018; Revised: June 3, 2018; Accepted: June 29, 2018

Abstract: The α-Fe_2O_3@SiO_2 reddish pigments with core–shell structure were successfully prepared by hydrothermal and Stöber methods. The structure, morphology, and chromaticity of the synthesized pigments were characterized by XRD, SEM, TEM, FTIR, XPS, and colorimetry. The results indicated that the as-prepared pigments have the characteristics of narrow particle size distribution, high dispersion, and good sphericity. The α-Fe_2O_3@SiO_2 reddish pigments were uniform and well dispersed in solution. In addition, the pigments with different shell thickness were also prepared, and the effect of shell thickness on the color performance of the pigments was discussed.

Keywords: Fe_2O_3@SiO_2 pigments; core–shell structure; monodispersed; spherical

1 Introduction

Inorganic pigment plays an important role in the ceramic industry for its excellent thermal stability, strong tinting strength, and abundant chromaticity [1–3]. Since red is one of the three primary colors, the demand for inorganic red pigments is larger than other colors. As far as we know, the most commercially available red ceramic pigment is CdS_xSe_{1-x}@$ZrSiO_4$ due to bright red hue, but its shortcomings cannot be ignored. Not only do the pigments contain toxic metals that are harmful to the human body and environment [4–7], but also $ZrSiO_4$ requires high sintering temperature (more than 1200 ℃) for the solid state reaction [8]. Therefore, Ce_2S_3 has attracted attention as the rare earth-based inorganic pigment because of its non-toxicity and bright color [9–11]. Unfortunately, Ce_2S_3 would be decomposed at high temperature and release hydrogen sulfide (H_2S), which is a considerable challenge for the commercial application [11].

Hematite–silica pigments have a long history, which are a kind of environmentally friendly and low-cost heteromorphic pigments [12,13]. The solid state reaction is a conventional method to synthesize the hematite–silica pigments. However, the synthesized pigments have low encapsulation rate and large particle size, which restrict their application [14]. The hematite–silica pigments with low encapsulation rate usually have low tinting strength, because non-protected hematite is eroded by the glassy phase and reduced to magnetite (Fe_3O_4) [15]. Besides, the inclusion structure of the pigments will be destroyed during the ball milling process. In order to improve the encapsulation

* Corresponding author.
E-mail: wangca@mail.tsinghua.edu.cn

rate and monodispersity of hematite–silica pigments, wet-chemistry synthesis methods, such as sol–gel and co-precipitation methods, are applied to the related research [16,17]. Nevertheless, these methods can not treat the structure and morphology of the hematite–silica pigments at the same time.

The structure and morphology of the inclusion pigments are the key factors for their application, especially in the field of ceramic ink [18,19]. In order to prevent nozzle clogging and ceramic ink deposition, submicron pigments have been developed [19]. However, at present, the direct synthesis of nanoscale pigments is still too expensive to be transferred to large-scale production [20,21]. Previous studies have shown that nanoscale pigments can effectively improve the dispersion and coloring ability in the glaze [18,22–24]. Based on these considerations, the hematite–silica pigments with optimum particle size and shape are considered as a very promising research direction. Therefore, we present a facile method to prepare highly dispersed spherical Fe_2O_3@SiO_2 reddish pigments with core–shell structure by two steps. In this work, the monodispersed Fe_2O_3 nanoparticles (NPs) prepared by hydrothermal method is used as colorant.

2 Experimental

2. 1 Synthesis of the chromophore particles

The highly dispersed α-Fe_2O_3 nanoparticles were prepared by hydrothermal method. Firstly, 2.89 g of $FeCl_3·6H_2O$ and 3.39 g of Na_2CO_3 were added into 80 mL deionized water and mixed by stirring. Then, this orange solution was transferred into a stainless steel autoclave of 100 mL capacity after stirring for 15 min. The hydrothermal procedure was maintained at 180 ℃ for 8 h, and then cooled to room temperature. Lastly, the red precipitate was collected by centrifugation and sequentially rinsed with deionized water and ethanol for three times. The obtained sample was dried at 70 ℃ for 5 h.

2. 2 Preparation of the reddish α-Fe_2O_3@SiO_2 pigments with core–shell structure

The reddish pigments were prepared by Stöber method with the as-prepared α-Fe_2O_3 as chromophore particles and tetraethoxysilane (TEOS, AR) as silica source. 0.05 g of the as-prepared α-Fe_2O_3 and 0.5 g of polyvinyl pyrrolidone (PVP-30) were added into 100 mL deionized water, and then the homogeneous solution was obtained by ultrasonic treatment for 15 min. Subsequently, the solution was continuously stirred at room temperature for 12 h. The PVP-modified α-Fe_2O_3 was collected by repeated centrifugation and washed with deionized water and ethanol for three times. The as-obtained α-Fe_2O_3 was dispersed in 100 mL ethanol by ultrasound for 5 min until it was uniform, and further 0.5, 1.5, 2.5 mL of ammonia and 0.1, 0.3, 0.5 mL of tetraethoxysilane were added into the solution under constant stirring, respectively. The detailed experimental conditions of samples are listed in Table 1. The obtained solution was then stirred at room temperature for 6 h to form α-Fe_2O_3@SiO_2 NPs. The as-prepared α-Fe_2O_3@SiO_2 NPs were then dried at 70 ℃ for 12 h and calcined at 1000 ℃ for 1 h in air. Figure 1 shows the schematic of formation of α-Fe_2O_3@SiO_2 pigments with core–shell structure.

2. 3 Characterization

The X-ray diffraction (XRD) patterns of the α-Fe_2O_3 and pigments were characterized by Bruker D8-Advance diffractometer employing Ni-filtered Cu Kα radiation (λ = 0.154 nm) with 40 kV of working voltage. The morphology and microstructure of the samples were investigated by S-4800 scanning electron microscope (SEM) equipped with an energy-dispersive X-ray spectroscopy (EDS). High-resolution transmission electron microscopy (HRTEM) imaging and EDS mapping were carried out in JEOL JEM-1010/2010 transmission electron microscope. The compositions of the as-prepared samples were collected by Fourier transform infrared spectroscopy (FTIR) on a NOVA4000 infrared spectrum instrument. Particle size and distribution of the pigments were investigated by

Table 1 Preparation conditions of Fe_2O_3@SiO_2

Sample	Fe_2O_3 (g)	CH_3CH_2OH (mL)	$NH_3·H_2O$ (mL)	TEOS (mL)
1	0.05	100	0.5	0.1
2	0.05	100	1.5	0.3
3	0.05	100	2.5	0.5

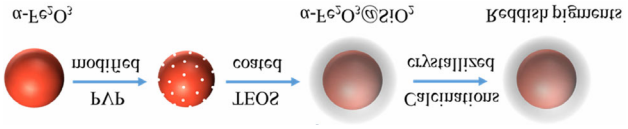

Fig. 1 Formation scheme for α-Fe_2O_3@SiO_2 reddish pigments.

Mastersizer 2000. The colorimetric parameters of the pigments were measured by YT-ACM402 automatic colorimeter based on the Commission Internationale de L'Eclairage (CIE) system, where L^* represents the lightness value on a scale of 0 (black) to 100 (white), and a^* and b^* the color opponents for green (–) to red (+) and blue (–) to yellow (+), respectively. The measurement conditions were included: an illuminant D65, 10° standard observer, and measuring geometry d/0°. C_{ab} (chroma) is defined as $C_{ab} = (a^{*2} + b^{*2})^{1/2}$, and purity of hue is 0–100.

3 Results and discussion

Based on the hydrothermal conditions in this work, the highly dispersed α-Fe_2O_3 nanoparticles were successfully synthesized. It could be seen that the as-prepared α-Fe_2O_3 exhibited monodispersity with spheroidic shape and narrow particle size distribution (the size is about 40 nm), as shown in Figs. 2(a) and 2(c). No obvious agglomeration phenomenon was observed. The phase of as-prepared α-Fe_2O_3 was confirmed by XRD (Fig. 2(b)); all the diffraction peaks can be well indexed to hexagonal phase of α-Fe_2O_3 (JCPDS No. 33-0664) without characteristic peaks of other crystalline phases. Besides, the HRTEM analysis results further demonstrate that the α-Fe_2O_3 nanoparticles are composed of high-purity single crystalline as shown in Fig. 2(d). The monodispersed cores contribute to the homogeneous inclusion and improve the dispersion of the core–shell particles. Therefore, the as-synthesized α-Fe_2O_3 nanoparticles are considered suitable as chromophore particles in the inclusion reddish pigments.

A dense coating is expected to be obtained to protect the α-Fe_2O_3 particles from being eroded by glassy phase at high temperature. So the morphology and microstructure of the as-synthesized α-Fe_2O_3@SiO_2 NPs were investigated and the results are presented in Fig. 3. The highly dispersed nanospheres with a particle size of around 200 nm were obtained without aggregation, as shown in Figs. 3(a) and 3(b). And the surface of nanospheres is smooth without holes. According to TEM image (Fig. 3(c)), the full core–shell structure can be seen, and chromophore particles are uniformly encapsulated in the shell of SiO_2 with a thickness of 60 nm. The EDS spectrum in Fig. 3(d) shows that the core–shell nanospheres are composed of O, Si, and Fe, whose fractions are about 39.4%, 57.4%, and 3.2%, respectively. On the other hand, the shell of different thickness can be obtained by changing the amount of TEOS. With the increase of

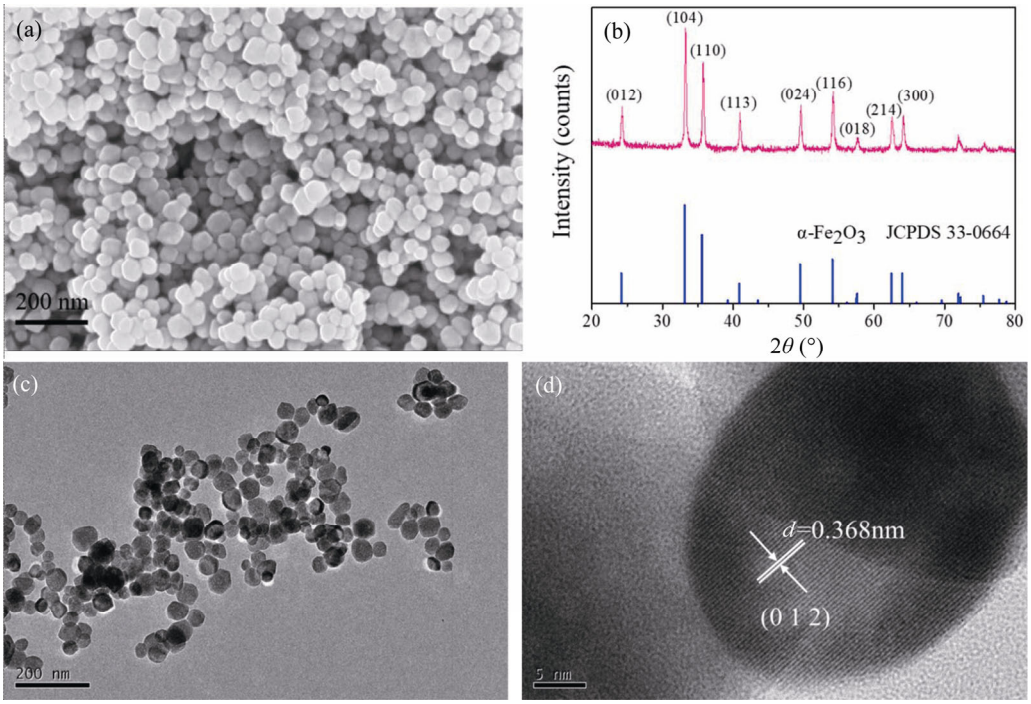

Fig. 2 (a) SEM image of the as-prepared α-Fe_2O_3 nanoparticles and (b) XRD pattern of the samples; (c) TEM and (d) HRTEM images of the samples.

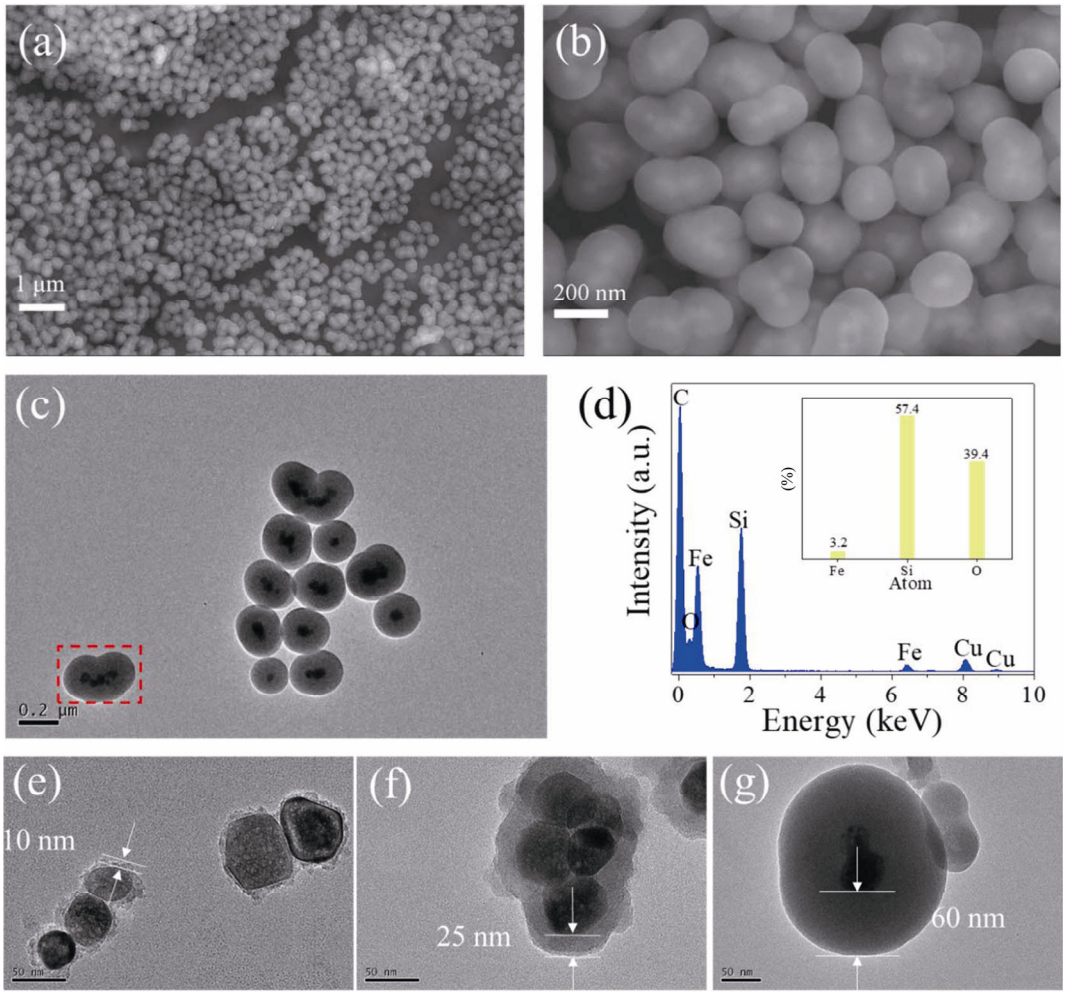

Fig. 3 (a, b) SEM micrographs of α-Fe_2O_3@SiO_2; (c) TEM micrograph and (d) EDS spectrum of α-Fe_2O_3@SiO_2 NPs; TEM images of α-Fe_2O_3@SiO_2 with the shell thickness of (e) 10 nm, (f) 25 nm, and (g) 60 nm.

TEOS addition, the shell thickness increases from 10 to 60 nm, as shown in Figs. 3(e)–3(g). The SiO_2 shell obtained by Stöber method is dense and non-porous with uniform thickness, and the chromophore particles can be well protected to achieve the effect of normal coloring. What is more, the α-Fe_2O_3@SiO_2 nanospheres with core–shell structure are almost monodispersed and homogeneous.

The phase and chemical state of the samples were investigated by XRD, FTIR, and XPS. Figure 4(a) shows the XRD patterns of the α-Fe_2O_3, α-Fe_2O_3@SiO_2 NPs, and α-Fe_2O_3@SiO_2 reddish pigments. After the formation of the core–shell structure, the diffraction peak of α-Fe_2O_3@SiO_2 NPs has a broad peak (2θ = 15°–25°), indicating the existence of amorphous SiO_2. After calcining at 1000 ℃, the diffraction peak at about 22° indicates that the amorphous silica shell is transformed into cristobalite phase and to form the reddish inclusion pigment [12,14]. Besides, the diffraction peak of α-Fe_2O_3 is obviously weakened after the formation of the core–shell structure. After calcination of α-Fe_2O_3@SiO_2 pigments, the intensity of the diffraction peak of α-Fe_2O_3 is further weakened. For comparison, the FTIR results of α-Fe_2O_3, α-Fe_2O_3@SiO_2 NPs, and α-Fe_2O_3@SiO_2 reddish pigments are presented in Fig. 4(b). Correspondingly, the bands at 3423.50 and 1627.85 cm^{-1} can be ascribed to the hydroxyl (–OH) stretching [25]. The peaks at 536.19 and 466.75 cm^{-1} are associated with the characteristic O–Fe–O bands for the α-Fe_2O_3 [26]. For the α-Fe_2O_3 coating by SiO_2, the bands at 1091.66 and 470 cm^{-1} arise from the O–Si–O bending and stretching vibration [25,26]. This suggests that the coating is formed on the surface of the α-Fe_2O_3 [26]. Moreover, the strength of the O–Si–O bond increases after the calcination, indicating the enhancement of interaction

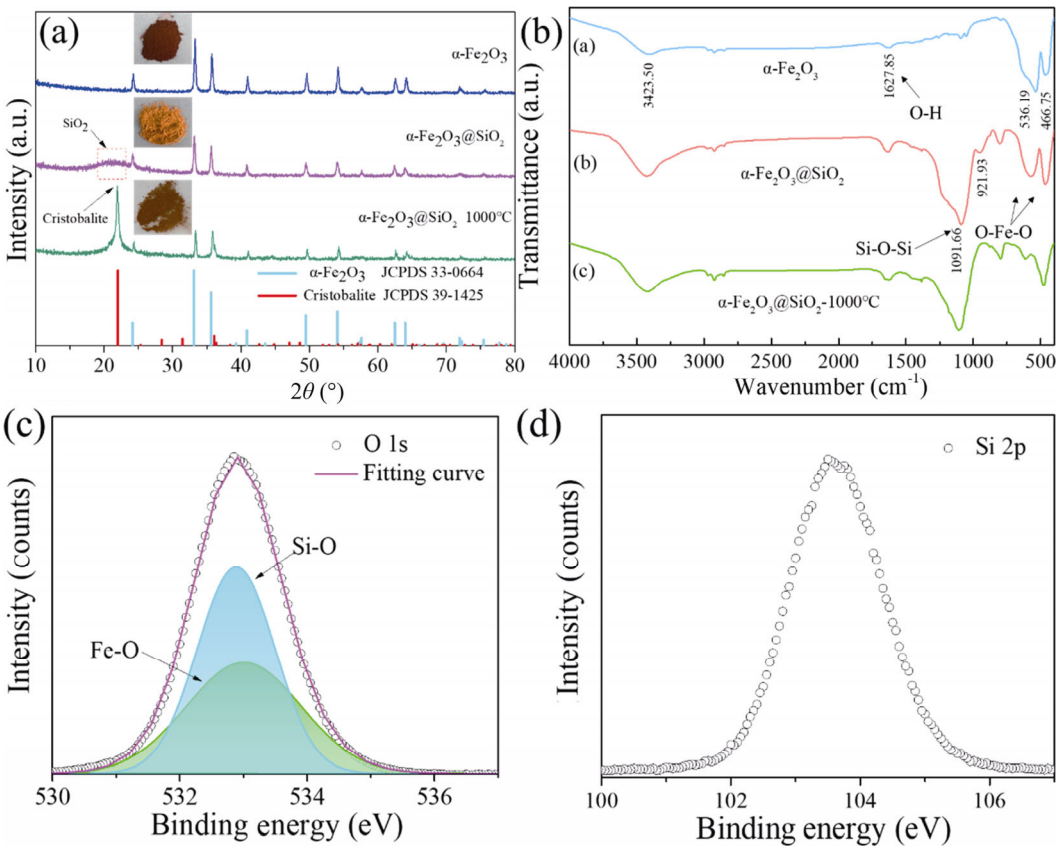

Fig. 4 (a) XRD patterns of the samples; (b) FTIR spectra of the samples; high-resolution XPS spectra of (c) O 1s and (d) Si 2p of the α-Fe_2O_3@SiO_2 pigments calcined at 1000 ℃.

between the core and the shell [26]. The reddish pigments were further analyzed by XPS, and the results are shown in Figs. 4(c) and 4(d). High-resolution XPS spectrum of O 1s confirms that Fe–O bonds and Si–O bonds exist in the pigment, as shown in Fig. 4(c) [25,27]. Meanwhile, new band can be observed at 103.5 eV in the Si 2p XPS spectrum, which is typical of Si in pure silica [27].

Moreover, the phase information for α-Fe_2O_3@SiO_2 pigments annealed at 600, 800, 1000 ℃ has been confirmed with XRD, as shown in Fig. 5. The XRD pattern of α-Fe_2O_3@SiO_2 pigments has a broad peak (2θ = 15°–25°) annealed at the temperature of 600 ℃. When the calcination temperature increases, amorphous SiO_2 transforms into cristobalite phase. And the narrow sharp peak at 22° suggests that the pigment is well crystallized under the temperature of 1000 ℃. In addition, all the diffraction peaks can be indexed to pure rhombohedral phase of α-Fe_2O_3 (JCPDS No. 33-0664). The results are consistent with the previous studies which also showed that the red shapes of pigments become poorer under higher calcination

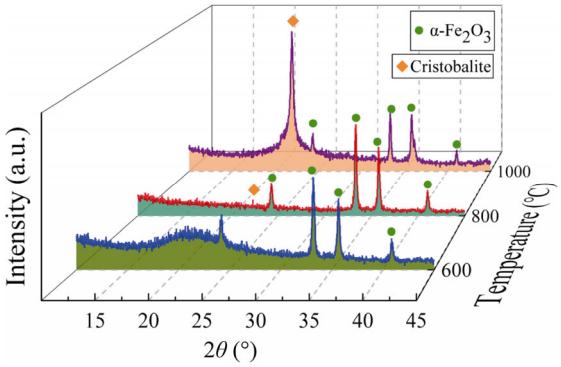

Fig. 5 XRD patterns of the α-Fe_2O_3@SiO_2 pigments with different calcination temperatures.

temperature (> 1000 ℃) [15]. Figures 6(a) and 6(b) present TEM and SEM images, respectively. It can be seen that the core–shell structure of the pigments is not destroyed and it remains high monodispersity. Most importantly, the α-Fe_2O_3@SiO_2 pigments also have the nanosphere morphology and narrow size distribution even in the absence of milling and sieving. In the industrial applications, a large amount of energy consumption can be saved and the damage to the core–

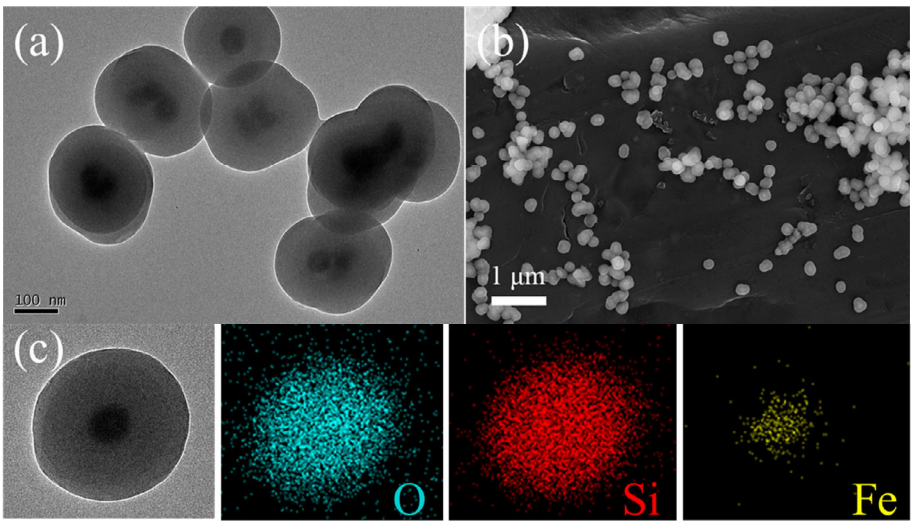

Fig. 6 (a) TEM and (b) SEM images of the α-Fe_2O_3@SiO_2 pigments with the shell thickness of 60 nm after calcination at 1000 ℃; (c) EDS mapping of the samples.

shell structure is avoided by ball milling. The EDS mapping of the pigments shows the locations of the different elements, and the core–shell structure of the pigments is obvious, as shown in Fig. 6(c). The particle size distribution of the α-Fe_2O_3@SiO_2 pigments is shown in Fig. 7. The average particle size of the α-Fe_2O_3@SiO_2 pigments with shell thickness of 60 nm is around 202.87 nm. In order to verify that the α-Fe_2O_3@SiO_2 pigments can meet the requirements of ceramic ink, we prepared the α-Fe_2O_3@SiO_2 ceramic ink by dispersion method and further put it on a desk for 72 h to check the stability. The composition of ceramic ink is shown in Table 2. It can be seen that the ceramic ink is stable after 72 h due to the α-Fe_2O_3@SiO_2 pigments with smaller particle size and better sphericity, as shown in Fig. 8.

Figure 9 shows the UV–Vis spectra of the α-Fe_2O_3 and α-Fe_2O_3@SiO_2 pigments with various shell thickness. It could see a typical absorption spectrum of α-Fe_2O_3. Two shoulders at 600–660 and 480–580 nm are attributed to the spin-forbidden $^6A_{1g}\rightarrow{}^4T_{2g}$ and $^6A_{1g}\rightarrow{}^4A_{1g}$ transitions of Fe^{3+} in octahedral environment, respectively. Furthermore, the color change of α-Fe_2O_3@SiO_2 pigments with the SiO_2 shell thickness was analyzed by the following equation:

$$E_g = 1240/\lambda_g$$

where E_g is the band gap energy of the sample and λ_g is the absorption wavelength. According to Fig. 9, λ_g values of samples (α-Fe_2O_3, α-Fe_2O_3@SiO_2 with shell thickness of 10, 25, and 60 nm) at the absorption edge are 620, 625, 650, 700 nm, respectively. Therefore, the

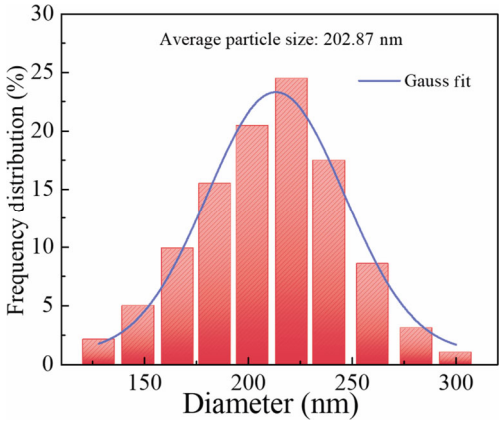

Fig. 7 Particle size distribution of the α-Fe_2O_3@SiO_2 pigments with shell thickness of 60 nm.

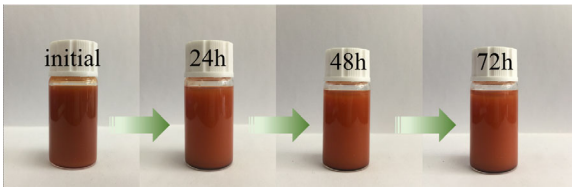

Fig. 8 Photographs of the ceramic ink after 24, 48, and 72 h.

corresponding band gap energies are 2, 1.98, 1.91, 1.77 eV, respectively. The band gap energy decreases with the increase of SiO_2 shell thickness [26]. Figure 10(a) illustrates the chromaticity coordinates compared to the 1931 CIE Standard Source C of the reddish pigments with various shell thickness. The coordinates of sample A are closer to red area than samples B, C, and D. And the colors of the samples from A to D are red, orange, and yellow, as shown in Fig. 10(b). The

Table 2 Composition of the α-Fe_2O_3@SiO_2 ceramic ink

Pigment	Solvent		Dispersant	Binder	Water
α-Fe_2O_3@SiO_2	1,2-Propylene glycol	Diethylene glycol	Butaedioic acid, sulfo-,1,4-diisooctyl ester, sodium salt	Styrene modified acrylate emulsion	43 wt%
30 wt%	10 wt%	5 wt%	7 wt%	5 wt%	

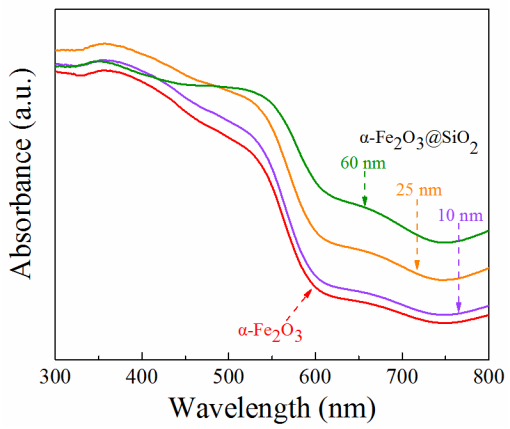

Fig. 9 UV–Vis spectra of the α-Fe_2O_3 and α-Fe_2O_3@SiO_2 pigments with various shell thickness.

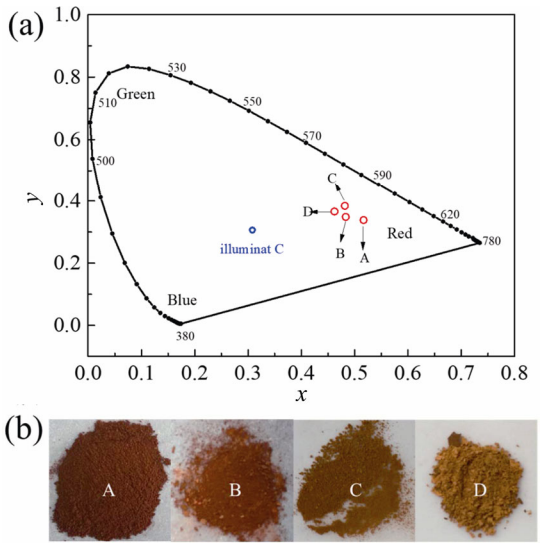

Fig. 10 (a) Chromaticity coordinates and (b) photograph of the α-Fe_2O_3@SiO_2 pigments with various shell thickness.

chromatic parameters of the pigments are listed in Table 3. With the increase of the shell thickness of SiO_2, L^* value of the pigment increases from 40.33 to 59.19, but a^* value decreases from 28.10 to 14.44. Meanwhile, the corresponding yellow–blue index increases from 15.91 to 34.47. Therefore, the introduction of SiO_2 shell improves the brightness and broadens the color of the pigment. In addition, the value of a^* decreases with the densification and crystallization of the SiO_2 shell after calcination.

Table 3 Chromaticity coordinates for the α-Fe_2O_3@SiO_2 pigments with various shell thickness

Sample	Shell thickness (nm)	L^*	a^*	b^*	C_{ab}
A	0	40.33	28.10	15.91	34.05
B	10	47.67	24.12	21.24	32.14
C	25	51.68	21.46	27.42	34.82
D	60	59.19	14.44	34.47	37.37
Non-calcined	60	57.89	15.79	33.11	36.68

4 Conclusions

In this paper, the α-Fe_2O_3@SiO_2 reddish pigments with core–shell structure were successfully prepared by hydrothermal and Stöber methods. The obtained pigments keep complete and dense coating layer on the basis of the nanoparticles. More importantly, excellent monodispersity and sphericity make the pigments meet the requirements of ceramic ink. On the other hand, the coating layer has a certain influence on the chromaticity performance of the pigments. With the increase of the thickness of the pigment shell, the brightness L^* value increases, while the redness a^* value decreases.

Acknowledgements

This work was financially supported by the Initiative Scientific Research Program from Jingdezheng Ceramic Institute and SRT Program (No. 1721T0264) from Tsinghua University.

References

[1] Guan L, Fan J, Zhang Y, *et al.* Facile preparation of highly cost-effective $BaSO_4$@$BiVO_4$ core–shell structured brilliant yellow pigment. *Dyes Pigments* 2016, **128**: 49–53.

[2] Bae B, Tamura S, Imanaka N. Novel environment-friendly yellow pigments based on praseodymium(III) tungstate. *Ceram Int* 2017, **43**: 7366–7368.

[3] Bae B, Wendusu, Tamura S, *et al.* Novel environmentally friendly inorganic yellow pigments based on gehlenite-type structure. *Ceram Int* 2016, **42**: 15104–15106.

[4] Jansen M, Letschert HP. Inorganic yellow-red pigments

without toxic metals. *Nature* 2000, **404**: 980–982.
[5] Yu S, Wang D, Gao X, *et al.* Effects of the precursor size on the morphologies and properties of γ-Ce_2S_3 as a pigment. *J Rare Earth* 2014, **32**: 540–544.
[6] Luo X, Zhang M, Ma L, *et al.* Preparation and stabilization of γ-La_2S_3 at low temperature. *J Rare Earth* 2011, **29**: 313–316.
[7] Roméro S, Mosset A, Macaudière P, *et al.* Effect of some dopant elements on the low temperature formation of γ-Ce_2S_3. *J Alloys Compd* 2000, **302**: 118–127.
[8] Cannio M, Bondioli F. Mechanical activation of raw materials in the synthesis of Fe_2O_3–$ZrSiO_4$ inclusion pigment. *J Eur Ceram Soc* 2012, **32**: 643–647.
[9] Yu S, Wang D, Liu Y, *et al.* Preparations and characterizations of γ-Ce_2S_3@SiO_2 pigments from precoated CeO_2 with improved thermal and acid stabilities. *RSC Adv* 2014, **4**: 23653–23657.
[10] Liu S-G, Li Y-M, Wang Z-M, *et al.* Enhanced high temperature oxidization resistance of silica coated γ-Ce_2S_3 red pigments. *Appl Surf Sci* 2016, **387**: 1147–1153.
[11] Mao W-X, Zhang W, Chi Z-X, *et al.* Core–shell structured Ce_2S_3@ZnO and its potential as a pigment. *J Mater Chem A* 2015, **3**: 2176–2180.
[12] Hosseini-Zori M. Substitution of a fraction of zircon by cristobalite in nano hematite encapsulated pigment and examination of glaze application. *J Adv Ceram* 2013, **2**: 149–156.
[13] Prim SR, Folgueras MV, de Lima MA, *et al.* Synthesis and characterization of hematite pigment obtained from a steel waste industry. *J Hazard Mater* 2011, **192**: 1307–1313.
[14] Hosseini-Zori M, Taheri-Nassaj E, Mirhabibi AR. Effective factors on synthesis of the hematite–silica red inclusion pigment. *Ceram Int* 2008, **34**: 491–496.
[15] Llusar M, Royo V, Badenes JA, *et al.* Nanocomposite Fe_2O_3–SiO_2 inclusion pigments from post-functionalized mesoporous silicas. *J Eur Ceram Soc* 2009, **29**: 3319–3332.
[16] Hosseini-Zori M, Bondioli F, Manfredini T, *et al.* Effect of synthesis parameters on a hematite–silica red pigment obtained using a coprecipitation route. *Dyes Pigments* 2008, **77**: 53–58.
[17] Opuchovic O, Kareiva A. Historical hematite pigment: Synthesis by an aqueous sol–gel method, characterization and application for the colouration of ceramic glazes. *Ceram Int* 2015, **41**: 4504–4513.
[18] He X, Wang F, Liu H, *et al.* Synthesis and coloration of highly dispersed $NiTiO_3$@TiO_2 yellow pigments with core–shell structure. *J Eur Ceram Soc* 2017, **37**: 2965–2972.
[19] Gardini D, Blosi M, Zanelli C, *et al.* Ceramic ink-jet printing for digital decoration: Physical constraints for ink design. *J Nanosci Nanotechnol* 2015, **15**: 3552–3561.
[20] Cavalcante PMT, Dondi M, Guarini G, *et al.* Colour performance of ceramic nano-pigments. *Dyes Pigments* 2009, **80**: 226–232.
[21] Gardini D, Dondi M, Luisa Costa A, *et al.* Nano-sized ceramic inks for drop-on-demand ink-jet printing in quadrichromy. *J Nanosci Nanotechnol* 2008, **8**: 1979–1988.
[22] Demarchis L, Sordello F, Minella M, *et al.* Tailored properties of hematite particles with different size and shape. *Dyes Pigments* 2015, **115**: 204–210.
[23] Legodi MA, de Waal D. The preparation of magnetite, goethite, hematite and maghemite of pigment quality from mill scale iron waste. *Dyes Pigments* 2007, **74**: 161–168.
[24] Völz HG. Comments on the development of tinting strength and ease of dispersion. *Prog Org Coat* 1990, **18**: 289–298.
[25] Peng C, Zhang C, Lv M, *et al.* Preparation of silica encapsulated carbon black with high thermal stability. *Ceram Int* 2013, **39**: 7247–7253.
[26] Zhang X, Liu Y, Li Y, *et al.* Preparation and thermal stability of the spindle α-Fe_2O_3@SiO_2 core–shell nanoparticles. *J Solid State Chem* 2014, **211**: 69–74.
[27] Pereira C, Pereira AM, Quaresma P, *et al.* Superparamagnetic γ-Fe_2O_3@SiO_2 nanoparticles: A novel support for the immobilization of [$VO(acac)_2$]. *Dalton Trans* 2010, **39**: 2842–2854.